A 14q distal chromoanagenesis elucidated by whole genome sequencing

Flavie Ader, Solveig Heide, Pauline Marzin, Alexandra Afenjar, Flavie Diguet, Sandra Chantot Bastaraud, Pierre-Antoine Rollat-Farnier, Damien Sanlaville, Marie-France Portnoï, Jean-Pierre Siffroi, et al.

A 14q Distal Chromoanagenesis elucidated by whole genome sequencing.

Flavie Ader [a*], Solveig Heide [a], Pauline Marzin[a], Alexandra Afenjar [b], Flavie Diguet [c,e], Sandra Chantot Bastaraud [a], Pierre-Antoine Rollat-Farnier [c,d], Damien Sanlaville [c,e], Marie-France Portnoï [a], Jean-Pierre Siffroi,[a], Caroline Schluth-Bolard [c,e]

[a] Sorbonne Université, Physiopathologie des Maladies Génétiques d'Expression Pédiatrique, F-75012 Paris, France.

[b] Unité de neuropédiatrie et pathologie du développement, GHU Paris Est - Hôpital d'Enfants Armand-Trousseau

[c] Service de Génétique, Laboratoire de Cytogénétique Constitutionnelle, Hospices Civils de Lyon, Bron, France

[d] Cellule bioinformatique de la plateforme NGS, Hospices Civils de Lyon, Bron, France

[e] GENDEV Team, Neurosciences Research Center of Lyon, INSERM U1028; CNRS UMR5292; UCBL1, 69677 BRON, France

*** Corresponding author**: flavie.ader@aphp.fr

ABSTRACT

Chromoanagenesis represents an extreme form of genomic rearrangements involving multiple breaks occurring on a single or multiple chromosomes. It has been recently described in both acquired and rare constitutional genetic disorders. Constitutional chromoanagenesis events could lead to abnormal phenotypes including developmental delay and congenital anomalies, and have also been implicated in some specific syndromic disorders. We report on a girl presenting with growth retardation, hypotonia, microcephaly, dysmorphic features, coloboma, and hypoplastic corpus callosum. Karyotype showed a *de novo* structurally abnormal chromosome 14q31qter region. Molecular characterization using SNP-array revealed a complex unbalanced rearrangement in 14q31.1-q32.2, on the paternal chromosome 14, including thirteen interstitial deletions ranging from 33kb to 1.56Mb in size, with a total of 4.1 Mb in size, thus suggesting that a single event like chromoanagenesis occurred. To our knowledge, this is one of the first case of 14q distal deletion due to a germline chromoanagenesis. Genome sequencing allowed the characterization of 50 breakpoints, leading to interruption of 10 genes including *YY1* which fit with the patient's phenotype. This precise genotyping of breaking junction allowed better definition of genotype-phenotype correlations.

KEY WORDS

chromoanagenesis; constitutionnal; intellectual disability; microcephaly; 14q deletion; coloboma; hypoplastic corpus callosum; genome sequencing

Introduction

Constitutional complex chromosome rearrangements (CCRs) are rare structural anomalies characterized by three or more breakpoints, involving at least a chromosome [1]. They are usually identified by standard karyotyping and further characterized by array-based analysis. Recently, highly complex changes termed chromoanagenesis, arising from shattering mechanisms, were observed in cancer genomes, and have also been described in rare patients with developmental disorders. Genomic imbalances included deletions, duplications and /or triplications, translocations and inversions, concentrated on a single or few chromosomes [2, 3, 4 ,5]. Depending of the mechanism of chromoanagenesis, several terms are used, chromotripsis referred to a mitotic event with chromosome shattering and non-homologous end joining repair; and chromoanasynthesis referred to a local defective DNA replication with microhomology-mediated template switching that produces local rearrangements with altered gene copy numbers. The presence of chromoanagenesis in healthy individuals affecting reproduction has also recently been reported [6, 7].

Here, we describe a complex 14q distal deletion consistent with a constitutional chromoanagenesis process, in a girl with developmental delay and congenital anomalies. Our patient shows clinical findings described in patients with 14q terminal deletion syndrome (developmental delay, hypotonia, growth retardation, microcephaly, a characteristic facial appearance and a variety of ocular anomalies, including retinal pigmentary changes, microphthalmia and coloboma) [8], especially ocular and brain malformations. The complexity of this case of chromoanagenesis, as well as the possibility to identify new genotype-phenotype relationships, has been elucidated by whole genome sequencing.

Clinical Report

The proband, an 8 month-old-girl, is the third child of healthy unrelated 42 years old mother and 38 years old father. The family history was negative for birth defects or developmental delay. The pregnancy had been complicated by maternal hypertension and intrauterine growth retardation (IUGR). Third trimester ultrasound examination revealed hypoplasia of the corpus callosum and reduction of the biparietal diameter. Cytogenetic analysis from amniotic cells performed in another institution showed an apparent normal 46,XX karyotype. She was born at 33+2 weeks of gestation after a caesarian section. Birth weight was 2050 g (< 3rd centile), birth length 43 cm (< 3rd centile) and head circumference 32 cm (3rd centile). After birth, she was hospitalized for one month because of hypotonia, feeding difficulties and growth retardation. Subsequently, hypertonic movements of the limbs were noted. At the age of 8 months, the neurological examination revealed axial hypotonia and peripheral hypertonia. She was unable to hold her head and to sit without support. She was not able to vocalize. She had a height of 60 cm (-3SD), a weight of 5100 g (-3SD), a microcephaly with a head circumference of 39 cm (-3SD) and a large anterior fontanel. Facial dysmorphic features included a broad and flat nasal bridge, epicanthus, a short nose, a broad philtrum, a small mouth with thin upper lip, and small and low-set ears. An electroencephalogram (EEG) gave normal results. Brain Magnetic resonance imaging (MRI) confirmed the corpus callosum hypoplasia. Ophthalmologic examination revealed bilateral chorioretinal coloboma. Echocardiography and renal ultrasound examination gave normal results. The patient died after a severe rhabdomyolysis event associated with multiorgan failure at the age of 2 years.

Investigations and Results

Cytogenetic analysis was performed again in our laboratory on GTG an RHG-banded metaphases from lymphocytes at a resolution of approximately 500 bands

95 according to the standard cytogenetic protocol (Fig. 1.A). FISH analyses using WCP
96 14 Probe (Metasystem, Altlussheim, Germany), tel 14q probe (Vysis, Illinois, Unated
97 States) and bacterial artificial chromosome (BAC) probes targeting the rearranged 14q
98 region, were realized according to standard procedures (Fig.1.B,C,D). Single
99 nucleotide polymorphism (SNP) microarray analysis was performed using a Human
100 OmniExpress24, which contains 713,599 markers including 395,094 SNPs (Illumina,
101 San Diego, United States), according to the manufacturer's protocol. Results were
102 analyzed with Illumina GenomeStudio software. SNP profiles were analyzed by
103 comparing the Log R ratio, i.e., ln (sample copy number/ reference copy number), and
104 the B allele frequency (BAF) (Fig 1.E,F). Data analysis was based on information from
105 the UCSC Genome Browser (NCBI37 hg19).
106 G-banded chromosomes analysis revealed an abnormal female karyotype with
107 structural changes spanning the terminal region of the long arm of one chromosome
108 14, in all the cells examined (Fig.1). Parental karyotypes were normal. Methylation
109 specific PCR of the differentially methylated region at 14q32 showed normal biparental
110 inheritance and no abnormality of methylation at the *GTL2/DKL1* region, confirming
111 that the patient does not have chromosome 14 uniparental disomy (UPD). SNP array
112 analysis revealed thirteen interstitial deletions of chromosome 14, between bands
113 14q31.1 and 14q32.2 (chr14: 83088298_100452660), ranged from 33 kb to 1.56 Mb
114 in size, with a total of 4.1 Mb in size (Fig.1, supplemental data 1). These deletions were
115 separated by normal copy number segments. The distal breakpoint was located at
116 740kb from the imprinted gene cluster. FISH analysis using BACs RP11-300J18
117 (14q31.3: 88484949_88502663) (Fig.1), RP11-543C4 (14q32.2:
118 100070893_100092077) confirmed the deletions. The BAC RP11-433J8 (14q32.2:
119 97059105_97061097) probe was not deleted. SNP-array analysis of deletions intervals

120 in the parents and patient revealed that the rearrangement derived from the paternal
121 chromosome 14 (supplemental data 2).
122 For a better understanding of the mechanism of this event, whole genome sequencing
123 (WGS) with break point analysis has been performed. A 350-bp fragments library was
124 prepared following the Illumina TruSeq DNA PCR-free protocol (Illumina, San Diego,
125 California, USA) with 3µg genomic DNA, according to manufacturer instructions. DNA
126 library was sequenced on an Illumina NextSeq 500 as paired-end 101 bp reads using
127 the High Output (300 cycles) NextSeq500 kit, yielding a mean sequencing depth of
128 14.32X. Image analysis and base calling were performed using Illumina Real Time
129 Analysis Pipeline 2 with default parameters. Alignment of the reads against the hg19
130 version of the human genome was done using BWA-MEM v 0.7.10 [9]. The reads were
131 sorted using Samtools v 1.3.1 [10], and the duplicates removed by PicardTools v 1.138
132 (picard.sourceforge.net). Structural variants (SV) were detected using BreakDancer v
133 1.4.5 [11] and annotated using an in-house program in order to filter out recurrent
134 variants. Integrative Genomics Viewer v 2.3 [12] was used for the SV visualization and
135 validation. Junction sequences were determined using split-read sequences when at
136 least 2 split-reads were available. If not possible, junction fragments were amplified by
137 PCR (junctions n°2, 6, 16, 20, 27, 28, 30, 41 and 46), in the patient and a control with
138 no chromosomal rearrangement, using Taq DNA Core kit 10 (MP Biomedicals, Solon,
139 Ohio), according manufacturer instructions followed by Sanger sequencing. Junctions
140 sequences were then aligned using BLAT tool (UCSC) against hg19 reference in order
141 to obtain the breakpoint at the base-pair level. WGS identified a highly complex
142 rearrangement including 50 breakpoints on chromosome 14, clustered in the
143 14q31.1q32.33 region. In 8 breakpoints (n°2, 6, 16, 20, 27, 28, 41 and 46), we
144 observed insertions of 3 to 9 small fragments (19-177 bp) derived from various

145 chromosomes (1,2,3,4,5,6,7,8,11,12,14,15,16,17 and 22) (Fig.2 and 3, supplemental
146 data 1 and 3), resulting in 35 small inserted fragments. Taken these small insertions
147 into account, this rearrangement resulted in 85 junctions. Twenty-three fragments of
148 chromosome 14 were in an inverted orientation, as well as 18/35 small inserted
149 fragments. We observed 2 to 7 bp microhomology (≥ 2bp) in 25/85 junctions. There
150 were twenty-one deletions on chromosome 14 (from 723 bp to 1565077 bp)
151 concordant with microarray analysis results (Fig.2). Besides these deletions, the
152 rearrangement disrupted 10 OMIM genes (*FLRT2*, *EML5*, *FOXN3*, *RPS6KA5*,
153 *CCDC88C*, *UNC79*, *SERPINA3*, *CLMN*, *GSKIP*, *YY1*).
154

155 **Discussion**

156 This case highlights the increasing complexity in genetic analysis and the fact that the
157 different steps complement each other. Although karyotype is not considered any more
158 as the first line laboratory examination in children presenting with developmental
159 defects and/or intellectual disability, many laboratories continue to perform standard
160 chromosome analysis, in parallel with molecular techniques like SNP-Array or next-
161 generation sequencing, since it allows the rapid diagnosis of most balanced
162 chromosomal rearrangements. When associated with an abnormal phenotype, these
163 latter are of importance in the identification of new genes responsible for these
164 pathologies. This strategy, from karyotype to NGS, is still justified since whole genome
165 sequencing is not yet widely available in current diagnosis.
166 In our patient, karyotyping revealed that one chromosome 14 showed an unusual
167 banding pattern on the long arm, thus leading to further investigations by SNP array. It
168 allowed to detect 13 deletions and to confirm the *de novo* occurrence of the event on
169 the paternal chromosome. However, deleted and interrupted genes, as identified by

170 this technique, didn't explain fully the phenotype of the patient suggesting that the
171 situation was more complex than expected and needing more sensitive methods like
172 Next Generation Sequencing (NGS).
173 Therefore, whole genome sequencing (WGS) was conducted and breakpoint cloning
174 identified 50 breakpoints and insertions of fragments involving 15 different
175 chromosomes, thus allowing a better characterization of this rearrangement and new
176 relationships between genes and the patient's phenotype.
177 Usually, chromoanagenesis in the context of congenital disorders involves one
178 or few chromosomes [5]. In our case, NGS revealed dramatically complex chromosomal
179 events since it involved 15 different chromosomes. Regarding to the chromotripsis
180 mechanism, firstly by analyzing ten constitutional CCRs, Kloosterman et al. (2012)
181 concluded that chromosome shattering by multiple DSBs and non-homologous repair
182 may be a common mechanism underlying chromothripsis rearrangements [13]. More
183 recently, Zhang et al. [14] demonstrated that the mechanism for chromothripsis can
184 involve the fragmentation and subsequent reassembly of a single chromatid from a
185 micronucleus, providing an explanation for the restriction of chromothriptic
186 rearrangements to a single chromosome.
349 We showed that the rearrangement had occurred *de novo* on the paternal
350 chromosome 14. This is in agreement with previous reports that demonstrated the
351 occurrence of this kind of events in the germline, as well as a paternal bias for CNV or
352 CCR formation [17,18]. The deletions, insertions and inversion pattern identified in this
353 case approached the pattern reported by Nazaryan-Petersen et al, and reinforced the
354 probability of a chromotripsis mechanism.[19]
355 Owing to data obtained from both SNP-array and WGS in our patient, we were able to
356 establish valuable genotype-phenotype correlations. In the literature, few patients with

357 pure terminal deletions of 14q, with or without ring chromosome formation, and
358 characterized by molecular cytogenetic methods have been reported [20,21,8]. A recurrent
359 1.11 Mb microdeletion of 14q32.2 including the *DLK1/GTL2* imprinted gene cluster,
360 mediated by expanded TGG repeats, has also been described in two unrelated
361 patients presenting with clinical features compatible with UPD (14)mat [22]. In our report,
362 the imprinted region on 14q was not involved, as determined by SNP-array and this
363 finding was confirmed by direct analysis of the methylation profile of the *DLK1/GTL2*
364 region (data not shown). Typical clinical features of the 14q terminal deletion syndrome
365 include developmental delay, hypotonia, growth retardation, microcephaly, a
366 characteristic facial appearance and a variety of ocular anomalies, including retinal
367 pigmentary changes, microphthalmia and coloboma [8]. Similar phenotypic features
368 were present in our patient, including chorioretinal coloboma. The structural eye
369 defects, microphthalmia, anophthalmia and coloboma (MAC) have a large genetic
370 component with several loci of genes located in the proximal and central parts of the
371 14q arm [8]. Review of the literature suggests that an additional locus for coloboma may
372 map to the terminal region of 14q32.31 [8 21]. In our case, the deleted regions, although
373 in the vicinity of the MAC spectrum locus, do not overlap with it but could have position
374 effects altering the expression of intact genes near the breakpoints. Alternatively, as
375 suggested by Salter et al. (2016), the possibility of an underlying multigenic mechanism
376 could to be considered. Indeed, our patient was also presenting with a hypoplastic
377 corpus callosum. Agenesis or dysgenesis of the corpus callosum is a heterogeneous
378 condition, for which several different genetic causes are known. Interestingly, in the
379 literature, an abnormal corpus callosum had previously been reported in four patients
380 with a 14q32 deletion, suggesting that a gene involved in corpus callosum
381 development may map to this region [23]. A chromoanagenesis on chr 14 has been

382 reported in a patient with developmental delay, characterized by the deletion of 2.7 Mb
383 in 14q32.33 and the insertion of 4q32.3 into the long arm of chromosome 14.[24]
384 Developmental delay fit with our case, but no other phenotypical features were fitting
385 between the two cases.
386 In our patient, the deleted regions contain genes like *EML1*, encoding for Echinoderm
387 microtubule-associated protein-like 1 which is expressed in eye and associated to the
388 photoreceptor [25] or *CYP46A1*, encoding for cytochrom oxydase 46A1 which is involved
389 in brain cholesterol metabolism [26]. Loss of *CYP46A1*, which may play an important role
390 in brain tissue, may be responsible for the neurologicals disorders observed in patients
391 with 14q deletion [27]. In the inserted fragments, no argument (content, localization or
392 orientation) was found to explain the patient's phenotype. In addition, breakpoint
393 analysis by genome sequencing revealed the interruption of 10 genes: *EML5*, *FOXN3*,
394 *RPS6KA5*, c14orf159, *CCDC88C*, *UNC79*, *SERPINA3, CLMN, GSKIP, YY1*. This
395 latter encodes for a zinc-finger transcription factor involved normal development and
396 malignancy. Deletions of *YY1* have been associated with cognitive impairments,
397 behavioral alterations, intrauterine growth restrictions, feeding problems, and various
398 congenital malformations [28]. These features could correspond to the phenotype in our
399 patient but with less severe issues. However, although eyes abnormalities (strabism
400 and hypermetropia) have been reported in 3 patients in the cohort of Gabriele-de
401 Vriess syndrome, coloboma has not been associated with this syndrome.
402
403 In conclusion, this report highlights the complementarity of different genomic
404 investigation techniques leading to a better comprehension of the mechanism in CCR
405 events, therefore leading to a better genetic counselling to the families.
406

Acknowledgments

We thank the technical team of the cytogenetic laboratory for their excellent assistance.

410 **Legend**

411 **FIGURE 1**

412 **G-Banding, FISH and SNP array analyses.**

413 **A**: Representative pair of G-banded chromosome 14. The distal region of the q arm
414 showed an abnormal banding pattern on one chromosome (arrow). **B**: FISH using the
415 Whole Chromosome Painting Probe 14 (wcp14 spectrum green, Metasystem). **C**: FISH
416 using subtelomere 14q probe (spectrum orange, hg19, chr14:107,159,193-
417 107,268,415) and LSI TCR 14q11.2 probe (spectrum aqua) (Vysis), showing signals
418 on both 14 chromosomes. **D**: FISH using BAC RP11-300J18 (14q31.3) (spectrum red,
419 hg19, chromosome14:88,484,949-88,502,663) spanning one deleted region (308 K)
420 and 14qtel probe (spectrum green, hg19, chromosome 14:107,159,193-107,268,415,
421 Vysis) do not show red signal on the der(14q) chromosome (arrow). **E**: SNP-array
422 profile of the terminal region of the long arm of chromosome 14 showing 13 deletions
423 clustered at 14q31.1-q32.2. B allele frequency and logR ratio are shown in the upper
424 panel. Orange bands indicate deleted regions. **F**: Genome studio representation of the
425 rearranged region between 14q31.1 and 14q32.2 bands (chr14: 83,088,298-
426 100,452,660), and the OMIM deleted genes.

427

428 **FIGURE 2**

429 Circos plot issue from the WGS data, showing clustering of the breakpoints on
430 chromosome 14 and the involvement of 15 other chromosomes.

431

432 **FIGURE 3**: Example of breakpoint junction number 41 structure. On the left, schematic
433 representation of the recombined region, with the different chromosomes' regions
434 represented by different colors. On the right, the details of the junction, the underlined
435 nucleotides correspond to homology region.

436

437

438

439

440

441

442

443

444

445 Bibliography:

446 [1] Zhang F, Carvalho CM, Lupski JR. Complex human chromosomal and genomic
447 rearrangements. *Trends Genet* 2009; **25**: 298-307.
448 [2] Kloosterman WP, Guryev V, van Roosmalen M, Duran KJ, de Bruijn E, Bakker SC, et
449 al. Chromothripsis as a mechanism driving complex de novo structural rearrangements in the
450 germline. *Hum Mol Genet* 2011; **20**: 1916-1924.
451 [3] Liu P, Erez A, Nagamani SC, Dhar SU, Kołodziejska KE, Dharmadhikari AV, et al.
452 Chromosome catastrophes involve replication mechanisms generating complex genomic
453 rearrangements. *Cell* 2011; **146**: 889-903.
454 [4] Stephens PJ, Greenman CD, Fu B, Yang F, Bignell GR, Mudie LJ, et al. Massive
455 genomic rearrangement acquired in a single catastrophic event during cancer development. *Cell*
456 2011; **144**: 27-40.
457 [5] Masset H, Hestand MS, Van Esch H, Kleinfinger P, Plaisancié J, Afenjar A, et al. A
458 Distinct Class of Chromoanagenesis Events Characterized by Focal Copy Number Gains. *Hum*
459 *Mutat* 2016; **37**: 661-668.
460 [6] Pellestor F, Anahory T, Lefort G, Puechberty J, Liehr T, Hédon B, et al. Complex
461 chromosomal rearrangements: origin and meiotic behavior. *Hum Reprod Update* 2011; **17**: 476-
462 494.
463 [7] de Pagter MS, van Roosmalen MJ, Baas AF, Renkens I, Duran KJ, van Binsbergen E,
464 et al. Chromothripsis in healthy individuals affects multiple protein-coding genes and can result
465 in severe congenital abnormalities in offspring. *Am J Hum Genet* 2015; **96**: 651-656.
466 [8] Salter CG, Baralle D, Collinson MN, Self JE. Expanding the ocular phenotype of 14q
467 terminal deletions: A novel presentation of microphthalmia and coloboma in ring 14 syndrome
468 with associated 14q32.31 deletion and review of the literature. *Am J Med Genet A* 2016; **170A**:
469 1017-1022.
470 [9] H L. Aligning sequence reads,
471 clone sequences and assembly contigs with BWA-MEM.arXiv:1303.3997 [q-bio.GN]:
472 arXiv:1303.3997 [q-bio.GN] 2013.
473 [10] Li H, Handsaker B, Wysoker A, Fennell T, Ruan J, Homer N, et al. The Sequence
474 Alignment/Map format and SAMtools. *Bioinformatics* 2009; **25**: 2078-2079.
475 [11] Chen K, Wallis JW, McLellan MD, Larson DE, Kalicki JM, Pohl CS, et al.
476 BreakDancer: an algorithm for high-resolution mapping of genomic structural variation. *Nat*
477 *Methods* 2009; **6**: 677-681.
478 [12] Thorvaldsdóttir H, Robinson JT, Mesirov JP. Integrative Genomics Viewer (IGV): high-
479 performance genomics data visualization and exploration. *Brief Bioinform* 2013; **14**: 178-192.
480 [13] Kloosterman WP, Tavakoli-Yaraki M, van Roosmalen MJ, van Binsbergen E, Renkens
481 I, Duran K, et al. Constitutional chromothripsis rearrangements involve clustered double-
482 stranded DNA breaks and nonhomologous repair mechanisms. *Cell Rep* 2012; **1**: 648-655.
483 [14] Zhang CZ, Spektor A, Cornils H, Francis JM, Jackson EK, Liu S, et al. Chromothripsis
484 from DNA damage in micronuclei. *Nature* 2015; **522**: 179-184.
485 [15] Macera MJ, Sobrino A, Levy B, Jobanputra V, Aggarwal V, Mills A, et al. Prenatal
486 diagnosis of chromothripsis, with nine breaks characterized by karyotyping, FISH, microarray
487 and whole-genome sequencing. *Prenat Diagn* 2015; **35**: 299-301.
488 [16] Collins RL, Brand H, Redin CE, Hanscom C, Antolik C, Stone MR, et al. Defining the
489 diverse spectrum of inversions, complex structural variation, and chromothripsis in the morbid
490 human genome. *Genome Biol* 2017; **18**: 36.
491 [17] Hehir-Kwa JY, Rodríguez-Santiago B, Vissers LE, de Leeuw N, Pfundt R, Buitelaar
492 JK, et al. De novo copy number variants associated with intellectual disability have a paternal
493 origin and age bias. *J Med Genet* 2011; **48**: 776-778.

494 [18] Fukami M, Shima H, Suzuki E, Ogata T, Matsubara K, Kamimaki T. Catastrophic
495 cellular events leading to complex chromosomal rearrangements in the germline. *Clin Genet*
496 2017; **91**: 653-660.
497 [19] Nazaryan-Petersen L, Eisfeldt J, Pettersson M, Lundin J, Nilsson D, Wincent J, et al.
498 Replicative and non-replicative mechanisms in the formation of clustered CNVs are indicated
499 by whole genome characterization. *PLoS Genet* 2018; **14**: e1007780.
500 [20] Zollino M, Ponzi E, Gobbi G, Neri G. The ring 14 syndrome. *Eur J Med Genet* 2012;
501 **55**: 374-380.
502 [21] Engels H, Schüler HM, Zink AM, Wohlleber E, Brockschmidt A, Hoischen A, et al. A
503 phenotype map for 14q32.3 terminal deletions. *Am J Med Genet A* 2012; **158A**: 695-706.
504 [22] Béna F, Gimelli S, Migliavacca E, Brun-Druc N, Buiting K, Antonarakis SE, et al. A
505 recurrent 14q32.2 microdeletion mediated by expanded TGG repeats. *Hum Mol Genet* 2010;
506 **19**: 1967-1973.
507 [23] Schneider A, Benzacken B, Guichet A, Verloes A, Bonneau D, Collot N, et al.
508 Molecular cytogenetic characterization of terminal 14q32 deletions in two children with an
509 abnormal phenotype and corpus callosum hypoplasia. *Eur J Hum Genet* 2008; **16**: 680-687.
510 [24] Kato T, Ouchi Y, Inagaki H, Makita Y, Mizuno S, Kajita M, et al. Genomic
511 Characterization of Chromosomal Insertions: Insights into the Mechanisms Underlying
512 Chromothripsis. *Cytogenet Genome Res* 2017; **153**: 1-9.
513 [25] Korenbrot JI, Mehta M, Tserentsoodol N, Postlethwait JH, Rebrik TI. EML1 (CNG-
514 modulin) controls light sensitivity in darkness and under continuous illumination in zebrafish
515 retinal cone photoreceptors. *J Neurosci* 2013; **33**: 17763-17776.
516 [26] Lund EG, Xie C, Kotti T, Turley SD, Dietschy JM, Russell DW. Knockout of the
517 cholesterol 24-hydroxylase gene in mice reveals a brain-specific mechanism of cholesterol
518 turnover. *J Biol Chem* 2003; **278**: 22980-22988.
519 [27] Repnikova EA, Astbury C, Reshmi SC, Ramsey SN, Atkin JF, Thrush DL, et al.
520 Microarray comparative genomic hybridization and cytogenetic characterization of tissue-
521 specific mosaicism in three patients. *Am J Med Genet A* 2012; **158A**: 1924-1933.
522 [28] Gabriele M, Vulto-van Silfhout AT, Germain PL, Vitriolo A, Kumar R, Douglas E, et
523 al. YY1 Haploinsufficiency Causes an Intellectual Disability Syndrome Featuring
524 Transcriptional and Chromatin Dysfunction. *Am J Hum Genet* 2017; **100**: 907-925.
525

Figure 1

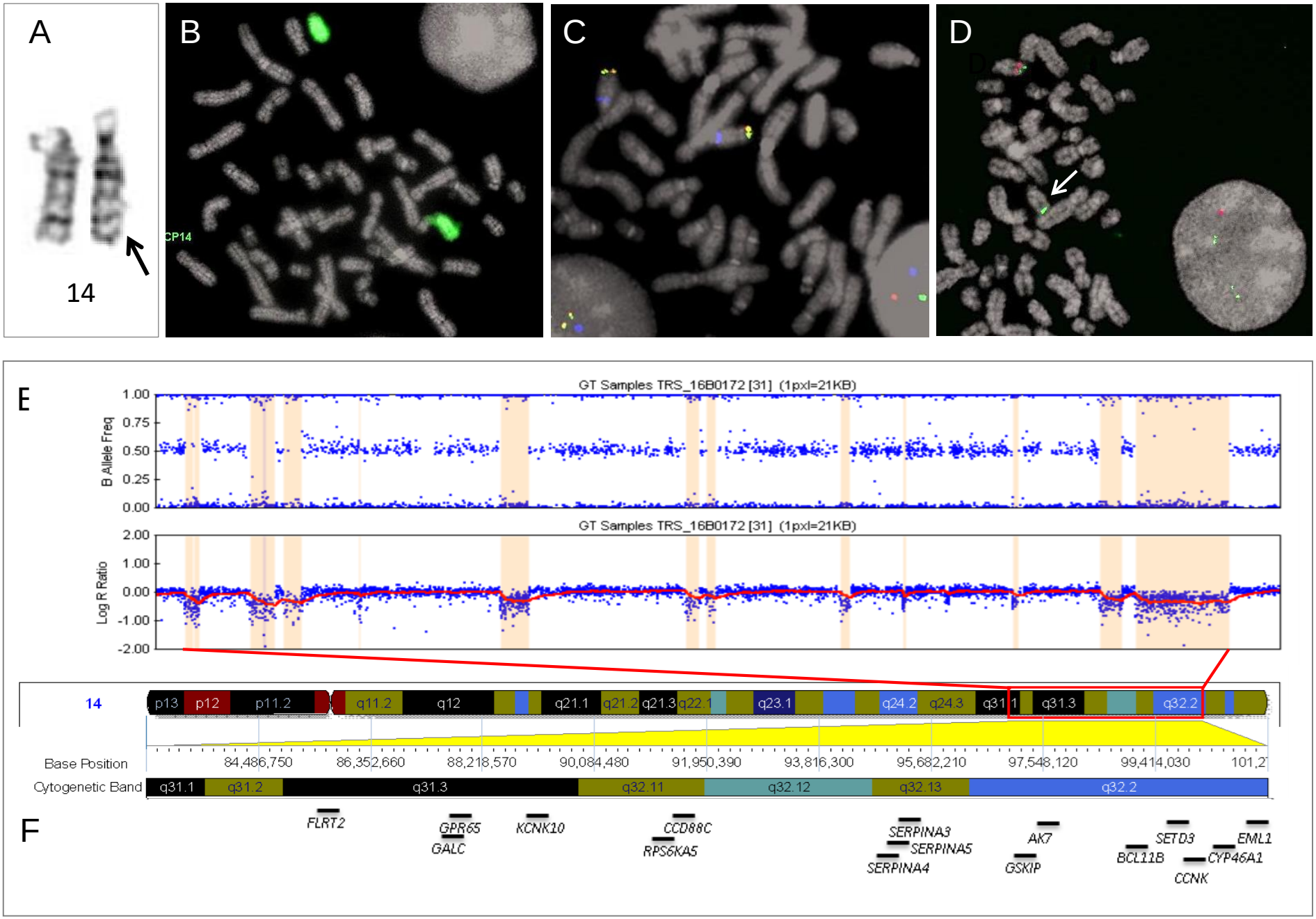
A
14
B
CP14
C
D
E
GT Samples TRS_16B0172 [31] (1pxl=21KB)
B Allele Freq
1.00
0.75
0.50
0.25
0.00
GT Samples TRS_16B0172 [31] (1pxl=21KB)
Log R Ratio
2.00
1.00
0.00
-1.00
-2.00
14
p13 p12 p11.2 q11.2 q12 q21.1 q21.2 q21.3 q22.1 q23.1 q24.2 q24.3 q31.1 q31.3 q32.2
Base Position
84,486,750 86,352,660 88,218,570 90,084,480 91,950,390 93,816,300 95,682,210 97,548,120 99,414,030
Cytogenetic Band
q31.1 q31.2 q31.3 q32.11 q32.12 q32.13 q32.2
F
FLRT2
GPR65
GALC
KCNK10
CCD88C
RPS6KA5
SERPINA3
SERPINA5
SERPINA4
AK7
GSKIP
SETD3
BCL11B
CCNK
CYP46A1
EML1

Figure 2

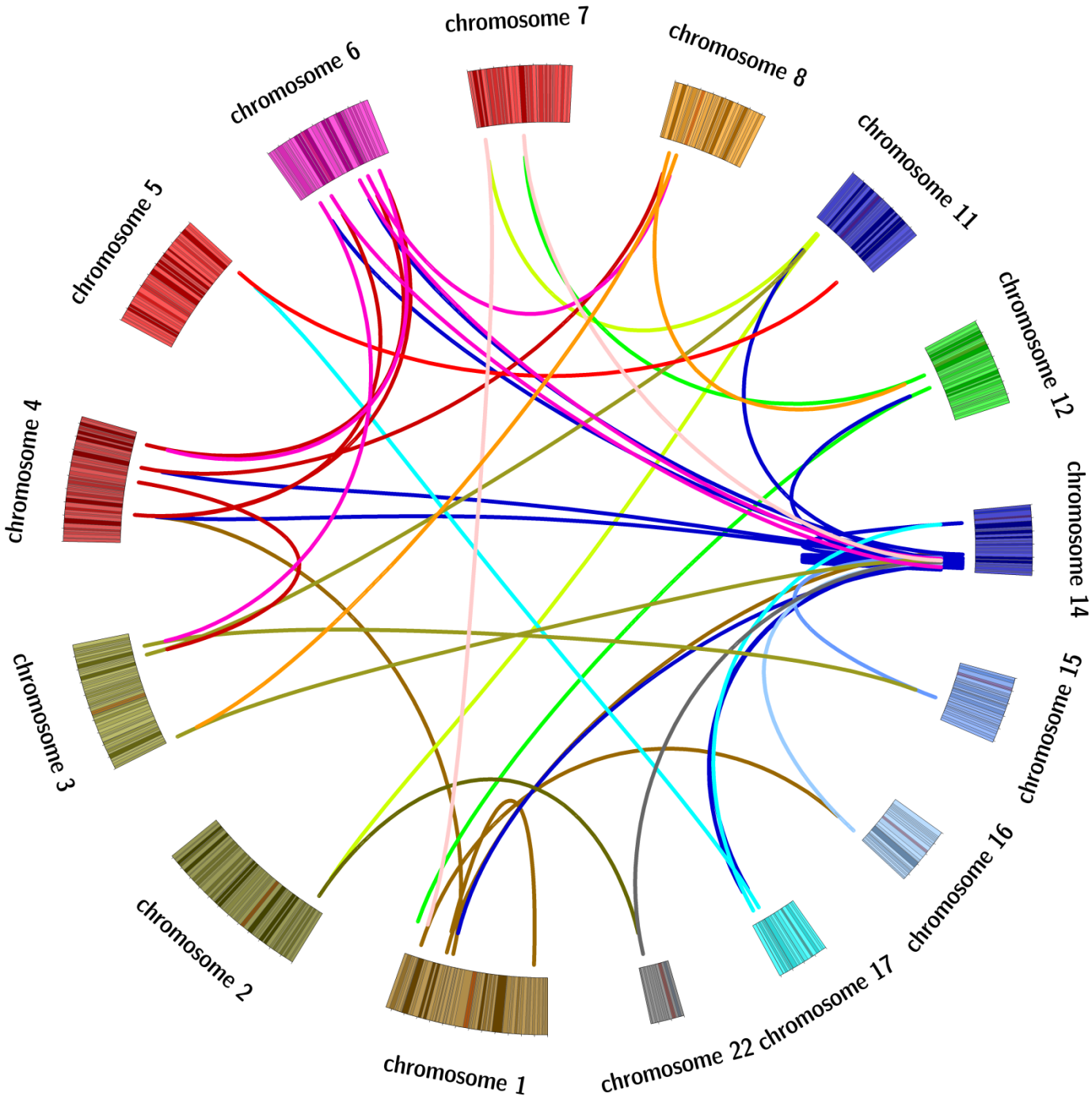
chromosome 1
chromosome 2
chromosome 3
chromosome 4
chromosome 5
chromosome 6
chromosome 7
chromosome 8
chromosome 11
chromosome 12
chromosome 14
chromosome 15
chromosome 16
chromosome 17
chromosome 22

Figure 3

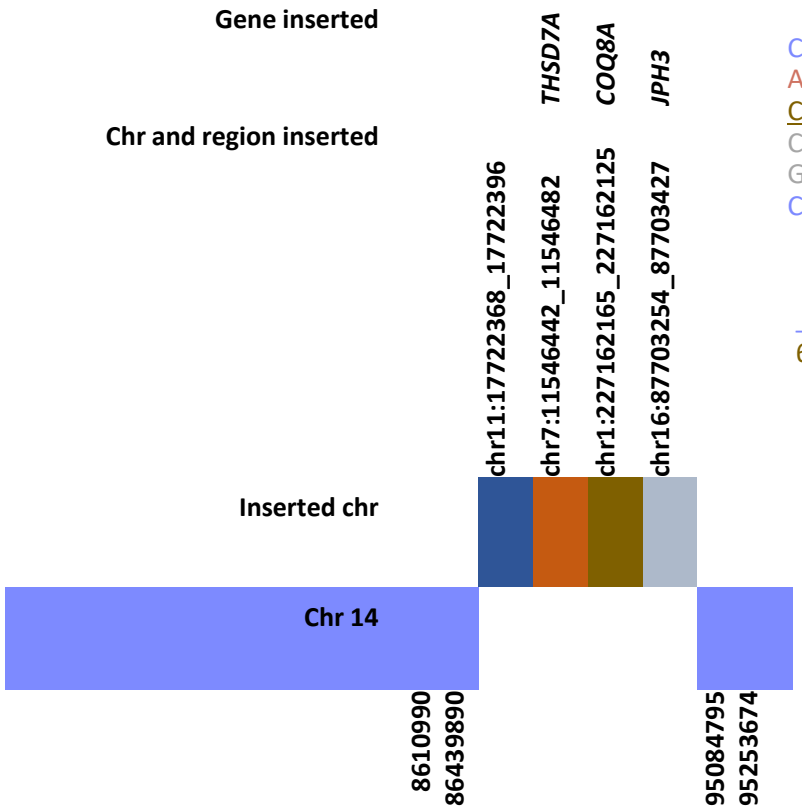

CTTCTCAAGGAGTACCTTTGCGGTCTTTATAAGTTCCTGTTATGGGCCAGACAACTTCTATCTTCCT
AGAGAGTCTTTGCATGACCCACCTGTCCTCACACCTCTCCCTGCTCAGATCCACATTCTAAGAGCGC
CTGGCGTGTGGGGTGGAGGCCGGGACAGTGTGAGGGCCGCCTGGTCAGAGCGGGAGGCAGGA
CCCCGTAGGGAGATGAAAGCCAAGCTGGACCCAGGCAGAAAAAGAGGAACGAAGGACAGGAA
GTCCAAGAGCAGTCACTGCTGACGTGAGTGCGGCCTGCAGGCAGCCAGTGTACTGAATCCAGGG
CAAATCTTAGCT

_chr14:86439890::chr11:17722368_17722396::chr7:11546442_11546482::chr1:227162165_227162125::chr16:87703254_87703427::chr14:95084795_